PHILOSOPHICAL TRANSACTIONS A

rsta.royalsocietypublishing.org

Research

Article submitted to journal

Subject Areas:
Physics

Keywords:
superconductivity, magnetism, Andreev bound states, Landau-Lifshitz-Gilbert equation, MAR, Shapiro steps

Author for correspondence:
Mikael Fogelström
e-mail:
mikael.fogelstrom@chalmers.se

Non-equilibrium charge and spin transport in SFS point contacts

C. Holmqvist[1], W. Belzig[2], and M. Fogelström[3]

[1]Department of Physics, Norwegian University of Science and Technology, NO-7491 Trondheim, Norway
[2]Fachbereich Physik, Universität Konstanz, D-78457 Konstanz, Germany
[3]Department of Microtechnology and Nanoscience - MC2, Chalmers University of Technology, SE-412 96 Göteborg, Sweden

The conventional Josephson effect may be modified by introducing spin-active scattering in the interface-layer of the junction. Here, we discuss a Josephson junction consisting of two s-wave superconducting leads coupled over a classical spin that precesses with the Larmor frequency due to an external magnetic field. This magnetically active interface results in a time-dependent boundary condition with different tunnelling amplitudes for spin-up and -down quasiparticles and where the precession produces spin-flip scattering processes. As a result, the Andreev states develop sidebands and a non-equilibrium population that depend on the details of the spin precession. The Andreev states carry a steady-state Josephson charge current and a time-dependent spin current, whose current-phase relations could be used for characterising the precessing spin. The spin current is supported by spin-triplet correlations induced by the spin precession and creates a feed-back effect on the classical spin in the form of a torque that shifts the precession frequency.

By applying a bias voltage, the Josephson frequency adds another complexity to the situation and may create resonances together with the Larmor frequency. These Shapiro resonances are manifested as torques and are, under suitable conditions, able to reverse the direction of the classical spin in sub-nanosecond time. Another characteristic feature is the subharmonic gap structure in the dc charge current displaying an even-odd effect that is attributable to precession-assisted multiple Andreev reflections.

THE ROYAL SOCIETY PUBLISHING

1. Introduction

Interesting spin phenomena may occur when ferromagnets are combined with superconductors (see [1] and [2] and references therein). Cooper pairs in a conventional superconductor have spin-singlet pairing which, if the superconductor is interfaced with a ferromagnet, extend into the ferromagnet. However, the exchange field inside the ferromagnet tries to align the two spins of the Cooper pairs and hence breaks the Cooper pairs apart resulting in a rapid decay of the superconducting correlations inside the ferromagnet. For the same reasons, the critical current of a Josephson junction with a ferromagnetic layer sandwiched between the two superconductors decays rapidly with increasing thickness of the ferromagnetic layer [3–6]. On the other hand, if weak ferromagnetic interfaces with magnetisation directions differing from the magnetisation direction of the ferromagnetic layer are inserted, the spin-singlet correlations may be transformed into spin-triplet correlations which can survive over a long range within the ferromagnet layer [7–11]. As a result of this non-collinear magnetisation of the ferromagnetic layer, the critical current decays similarly to a supercurrent in a non-magnetic metal with increasing junction length [12,13]. So far, the existence of spin-triplet correlations has been measured in this indirect way. A more direct way of detecting the spin-triplet correlations would be to measure the effects of the spin on the triplet correlations, e.g. by using phenomena explored in conventional spintronics such as spin-transfer torques and other means for creating magnetisation dynamics effects or magnetisation switching. There has been theoretical work done in this direction [14–16] using approaches based on the Bogoliubov-de Gennes equations [17–21] and Green's function methods [22–27] as well as some experimental work investigating the coupling between the dynamics of magnetic moments and Josephson currents [28,29], but to our knowledge there has been no experimental investigation of the coupling between magnetisation dynamics and induced triplet correlations. This is a crucial step in developing superconducting spintronics applications [2]. In this article, we will review recent work on how magnetisation dynamics of a nanomagnet couple to the induced spin-triplet correlations associated with the charge and spin Josephson effects, and discuss how the dynamic interactions between the induced spin-triplet correlations and the nanomagnet lead to non-equilibrium transport properties that can be used to probe the induced triplet correlations directly.

2. Quasiclassical model

Consider two ordinary BCS s-wave superconductors, with a phase difference φ, coupled over a nanomagnet as depicted in Fig. 1(a). The nanomagnet may be a magnetic molecule or a magnetic nanoparticle which we will treat as a classical spin, $\boldsymbol{S}$, with magnetic moment $\boldsymbol{\mu} = \gamma \boldsymbol{S}$, and the gyromagnetic ratio γ. The nanoparticle supports a few conduction channels when placed between the two metallic leads. If the nanomagnet is subjected to an external magnetic field, $\boldsymbol{H}$, it will precess when the effective field is applied at an angle, ϑ, relative to the spin. $\boldsymbol{H}$ is an effective field that includes any r.f. fields needed to maintain precession, crystal anisotropy fields and demagnetisation effects. The spin and the effective magnetic field couple via a Zeeman term, $\mathcal{H}_B = -\gamma \boldsymbol{S}(t) \cdot \boldsymbol{H}$. At finite tilt angle, ϑ, the spin precesses with the Larmor frequency, $\omega_L = \gamma H$, where $H = |\boldsymbol{H}|$ is the magnitude of the effective field. The spin dynamics are described by the Landau-Lifshitz-Gilbert equation of motion [30,31]

$$\frac{d\boldsymbol{S}}{dt} = -\gamma \boldsymbol{S}(t) \times \boldsymbol{H} + \boldsymbol{\tau}(t), \tag{2.1}$$

where the first term on the right-hand side is the torque produced by the effective field and the second term, $\boldsymbol{\tau}(t)$, is a torque that collects effects caused by the mutual coupling between the precessing nanomagnet and the superconducting quasiparticle system.

The coupling of the motion of the spin and the quasiparticle tunnelling over the spin enters via a time-dependent tunnelling term, $\hat{\mathcal{H}}_T = \hat{\psi}_L^\dagger \hat{v}_{LR}(t) \hat{\psi}_R + H.C.$, where $\hat{\psi}_\alpha$ is the usual spin-dependent Nambu-spinor that describes the superconducting state in lead $\alpha = \mathrm{R}, \mathrm{L}$. The hopping

matrix $\hat{v}_{LR}(t)\,(=\hat{v}^{\dagger}_{RL}(t)\equiv\hat{v}(t))$ has a spin-structure that may be parametrised into a spin-independent amplitude $\mathrm{v_o}$ and a spin-dependent amplitude $\mathrm{v_s}(t)$. It has the following matrix structure in the combined 4×4 Nambu-spin space,

$$\hat{v}_{LR}(t)=\begin{pmatrix}\mathrm{v_o}+\mathrm{v_s}(\boldsymbol{e}_S(t)\cdot\boldsymbol{\sigma}) & 0\\ 0 & \mathrm{v_o}-\mathrm{v_s}\sigma_y(\boldsymbol{e}_S(t)\cdot\boldsymbol{\sigma})\sigma_y\end{pmatrix}. \tag{2.2}$$

We use the time-dependent unit vector, $\boldsymbol{e}_S(t)$, along $\boldsymbol{S}(t)=|\boldsymbol{S}|\boldsymbol{e}_S(t)$ and include the magnitude $|\boldsymbol{S}|$ in the spin-dependent amplitude $\mathrm{v_s}$. Above, $\boldsymbol{\sigma}=(\sigma_x,\sigma_y,\sigma_z)$ with σ_i being the *i-th* Pauli matrix. The spin-independent amplitude and the portion of the spin-matrix parallel to $\boldsymbol{H}$, $\mathrm{v_o}+\mathrm{v_s}\cos\vartheta\,(\boldsymbol{e}_z\cdot\boldsymbol{\sigma})$, describe the tunnelling amplitudes for spin-up and spin-down quasiparticles, while the portion perpendicular to $\boldsymbol{H}$, $\mathrm{v_s}\sin\vartheta\,(\cos(\omega_L t)\boldsymbol{e}_x+\sin(\omega_L t)\boldsymbol{e}_y)\cdot\boldsymbol{\sigma}$, induces time-dependent spin flips. Our model is a generalisation to arbitrary tunnelling coupling of the one studied by Zhu and co-workers [25,32].

We use the quasiclassical theory of superconductivity [33–36] to solve the non-equilibrium tunnelling problem stated above. Within quasiclassical theory, interfaces are handled by the

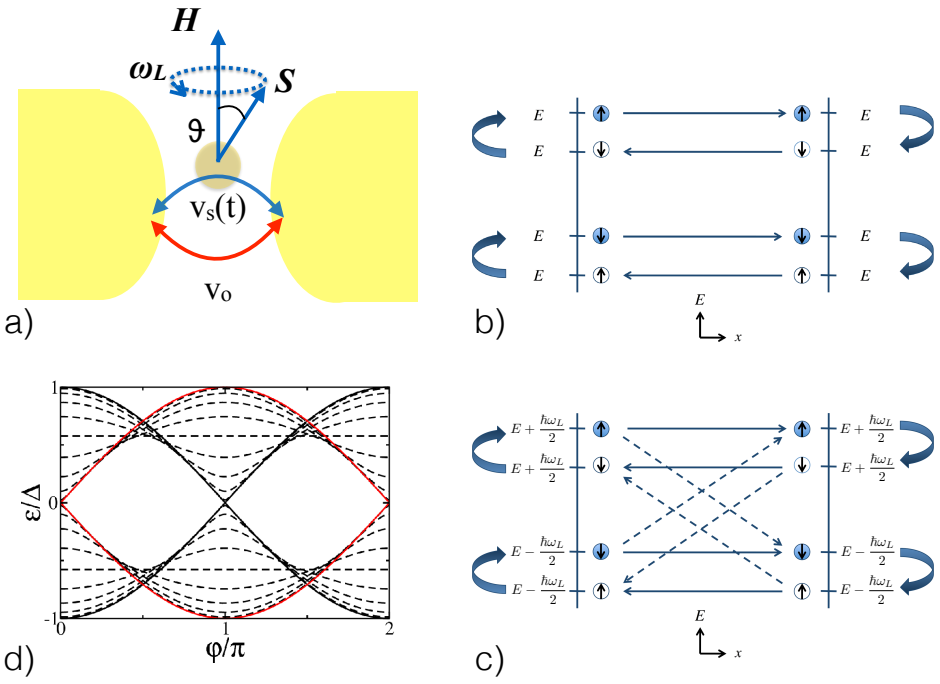

Figure 1. (a) Two superconducting leads are coupled over the spin of a nanomagnet. The tunnel junction is characterised by the hopping amplitudes $\mathrm{v_o}$ and $\mathrm{v_s}(t)$, where $\mathrm{v_o}$ is the spin-independent tunnelling and $\mathrm{v_s}(t)$ is the phenomenological time-dependent coupling generated by the nanomagnet, whose spin precesses with the frequency ω_L at the cone angle ϑ. (b) The schematics of conventional Andreev scattering between two superconductors at phase difference φ. Constructive interference occurs at a phase-dependent energy $\varepsilon(\varphi)$ defining two energy-degenerate Andreev levels. (c) In addition to the spin-conserving tunnelling (solid lines), the dynamics of the spin allows for tunneling processes with spin-flip scattering combined with an absorption or emission of the energy $\hbar\omega_L$ (dashed lines). The combination of these tunnelling processes results in a lifting of the spin-degeneracy of the Andreev levels in (b) and the appearance of time-dependent spin-triplet pairing amplitudes. (d) For a junction with a static spin, the Andreev-level spectrum's dependence on phase may be modified from a 0 junction, $\mathrm{v_o}>\mathrm{v_s}$, to a π junction, $\mathrm{v_o}<\mathrm{v_s}$. The black full line is $(\mathrm{v_o},\mathrm{v_s})=(1,0)$ and the red line is $(\mathrm{v_o},\mathrm{v_s})=(0,1)$. The dashed lines span between these two limits in increments of 0.1.

formulation of boundary conditions, which usually have been expressed as scattering problems [37–46]. In many problems, in particular when an explicit time dependence appears, we find the t-matrix formulation more convenient to use [47–49]. This formulation is also well suited for studying interfaces with different numbers of trajectories on either side as is the case for normal metal/half metal interfaces [50,51]. For a full account on how to solve the time-dependent boundary condition we refer to our original articles [52–55].

The quasiclassical propagator in lead α, $\check{g}_\alpha$, is a 2×2 matrix in Keldysh space, denoted by the check "$\check{}$". Each component is in turn a 4×4 matrix in the combined Nambu-spin space and has the general form

$$\hat{g}^{R,A,K} = \begin{pmatrix} g+\boldsymbol{g}\cdot\boldsymbol{\sigma} & (f+\boldsymbol{f}\cdot\boldsymbol{\sigma})i\sigma_y \\ i\sigma_y\,(\tilde{f}+\tilde{\boldsymbol{f}}\cdot\boldsymbol{\sigma}) & \sigma_y(\tilde{g}-\tilde{\boldsymbol{g}}\cdot\boldsymbol{\sigma})\sigma_y \end{pmatrix}^{R,A,K} \tag{2.3}$$

for the retarded (R), advanced (A), and Keldysh (K) components. To obtain $\check{g}_\alpha$ for a non-homogeneous system, we solve the transport equation

$$iv_F\partial_x\check{g}_\alpha(\hat{p}_F) + [\check{\varepsilon} - \check{\Delta}_\alpha, \check{g}_\alpha(\hat{p}_F)]_\circ = \check{j}_\alpha\delta(x-x_c)/(2\pi i) \tag{2.4}$$

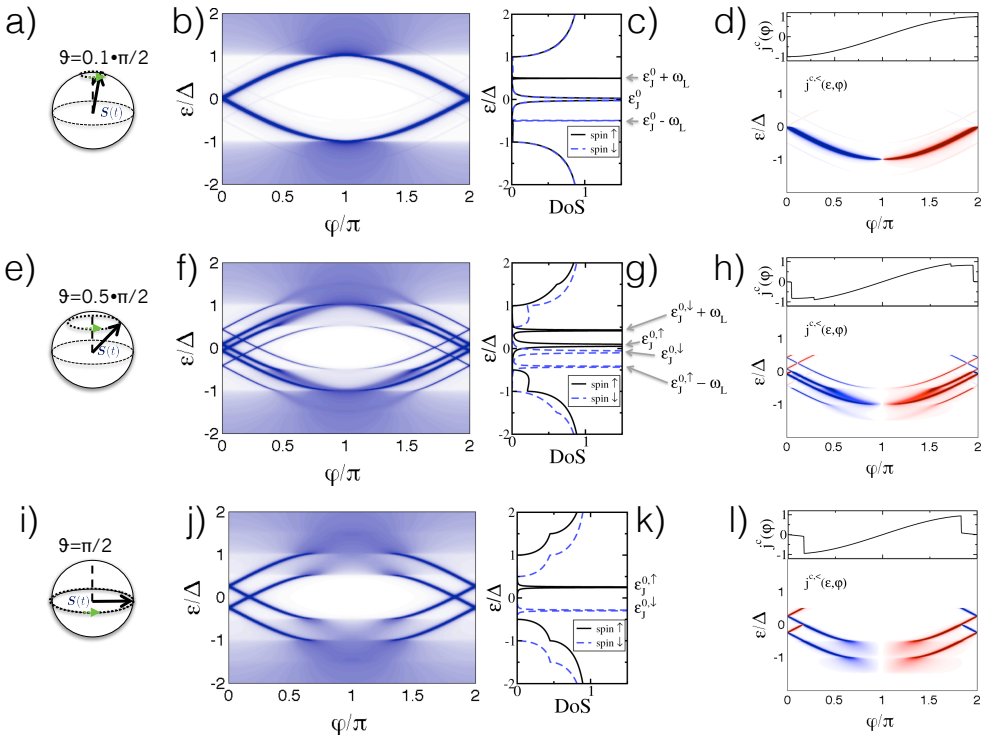

Figure 2. The Josephson effect over a precessing spin at frequency $\omega_L = 0.5\Delta$ for various cone angles (a-d) $\vartheta = 0.1\pi/2$, (e-h) $\vartheta = \pi/4$, and (i-l) $\vartheta = \pi/2$. The tunnelling parameters are $\mathrm{v_o} = 0, \mathrm{v_s} = 1$ and the temperature is $T = 10^{-5}\Delta$. The structure of the Andreev-level spectrum is shown vs. phase in panels (b,f,j) [56] and the density of states (DoS) at $\varphi = 0$ in (c,g,k) [53]. The current-phase relations, $j^c(\varphi)$, and the charge current kernels, $j^{c,<}(\varepsilon,\varphi)$, are shown in panels (d,h,l) [53]. $j^{c,<}(\varepsilon,\varphi)$ shows how the Andreev levels in (b,f,j) are populated and in which direction they carry current; red into the right and blue into the left lead. At some phase differences $\varphi_c < \varphi < 2\pi - \varphi_c$, scattering between the Andreev levels and the continuum states broadens the otherwise sharp in-gap states. The charge current (plotted in units of $e\Delta/\hbar$) is the energy-integrated spectral current and displays abrupt jumps at phase differences where Andreev levels become populated/unpopulated. The DoS at $\varphi = 0$ shows the splitting of the spin-up and spin-down Andreev levels as well as the scattering of the continuum levels into the gap.

along a trajectory $\hat{p}_F$ in lead α. The boundary conditions for the components of $\check{g}_\alpha$ enter via a localised inhomogeneity, given by the tunnel Hamiltonian, at the position of the contact, x_c [57–59]. The source term is a matrix current defined as $\check{j}_\alpha/2\pi i = [\check{t}_\alpha(\hat{p}_F,\hat{p}_F),\check{g}^0_\alpha(\hat{p}_F)]_\circ$. The $\circ$-product is a matrix multiplication and convolution over common time arguments and $\check{g}_\alpha$ additionally obeys a normalisation condition $\check{g}_\alpha\circ\check{g}_\alpha = -\pi^2\check{1}$. The matrix, $\check{t}_\alpha(\hat{p}_F,\hat{p}_F)$, solves the t-matrix equation

$$\check{t}_\alpha(t,t') = \check{\Gamma}_\alpha(t,t') + [\check{\Gamma}_\alpha\circ\check{g}^0_\alpha\circ\check{t}_\alpha](t,t'). \tag{2.5}$$

The t-matrix $\check{t}_\alpha$ depends on the hopping elements of Eq. (2.2) via a matrix $\check{\Gamma}_L(t,t')$ defined as $\check{\Gamma}_L(t,t') = [\check{v}\circ\check{g}^0_R\circ\check{v}](t,t')$ for the left side of the interface. The right-side matrix $\check{\Gamma}_R$ is correspondingly obtained from the left-side propagator $\check{g}^0_L$. $\check{g}^0_{L,R}$ are the bulk propagators in either lead computed without the tunnelling term. From the t-matrices (2.5), we calculate the full quasiclassical propagators, which can be separated into "incoming" ($\check{g}^i$) and "outgoing" ($\check{g}^o$) propagators depending on if their trajectories lead up to or away from the interface. These propagators are given by

$$\check{g}^{i,o}_\alpha(t,t') = \check{g}^0_\alpha(t,t') + [(\check{g}^0_\alpha \pm i\pi\check{1})\circ\check{t}_\alpha\circ(\check{g}^0_\alpha \mp i\pi\check{1})](t,t'), \tag{2.6}$$

where $\pm$ and $\mp$ refer to the incoming and outgoing propagators, respectively. The matrix currents give the charge and spin currents via

$$j^c_\alpha(t) = \frac{e}{2\hbar}\int\frac{d\varepsilon}{8\pi i}\mathrm{Tr}[\hat{\tau}_3\hat{j}^<_\alpha(\varepsilon,t)]; \tag{2.7a}$$

$$\boldsymbol{j}^s_\alpha(t) = \frac{1}{4}\int\frac{d\varepsilon}{8\pi i}\mathrm{Tr}[\hat{\tau}_3\hat{\boldsymbol{\sigma}}\hat{j}^<_\alpha(\varepsilon,t)], \tag{2.7b}$$

where $\hat{\tau}_3 = \mathrm{diag}(1,-1)$, $\hat{\boldsymbol{\sigma}} = \mathrm{diag}(\boldsymbol{\sigma},-\sigma_y\boldsymbol{\sigma}\sigma_y)$ and "$\hat{}$" denotes a 4×4 matrix in Nambu-spin space. The lesser ("$<$") propagators can be obtained as $\hat{g}^< = (1/2)(\hat{g}^K - \hat{g}^R + \hat{g}^A)$. The itinerant electrons generate a spin transfer torque which gives a contribution to the torque in Eq. (2.1) as $\boldsymbol{\tau} = \boldsymbol{j}^s_L - \boldsymbol{j}^s_R$.

The spin independence of $\check{g}^0_\alpha(\varepsilon)$ and the form of the hopping elements simplify the time-dependent problem. This simplification can be made due to the fact that the Keldysh-Nambu-spin matrices can be factorised in spin space into generalised diagonal matrices, $\check{X}_d$, spin-raising matrices, $\check{X}_\uparrow$, and spin-lowering matrices, $\check{X}_\downarrow$. In general, a matrix factorised in this form has the time dependence

$$\check{X}(t,t') = (2\pi)^{-1}\int d\varepsilon\, \mathrm{e}^{-i\varepsilon(t-t')}\left[\check{X}_d(\varepsilon,\omega_L) + +\mathrm{e}^{-i\omega_L t}\check{X}_\uparrow(\varepsilon,\omega_L) + \mathrm{e}^{i\omega_L t}\check{X}_\downarrow(\varepsilon,\omega_L)\right]. \tag{2.8}$$

The matrices $\check{X}_d$, $\check{X}_\uparrow$, and $\check{X}_\downarrow$ are still Keldysh-Nambu matrices and, in addition, obey the usual algebraic rules for spin matrices, i.e. $\check{X}_\uparrow\circ\check{Y}_\uparrow = \check{X}_\downarrow\circ\check{Y}_\downarrow = 0$, $\check{X}_{\downarrow,\uparrow}\circ\check{Y}_{\uparrow,\downarrow}\propto\check{Z}_d$, and $\check{X}_d\circ\check{Y}_{\uparrow,\downarrow}\propto\check{Z}_{\uparrow,\downarrow}$. Observables, such as the charge and spin currents above, will have the general time dependence

$$\mathcal{O}(t;\omega_L) = \mathcal{O}_o(\omega_L) + \mathcal{O}_z(\omega_L)\sigma_z + \mathcal{O}_\uparrow(\omega_L)\mathrm{e}^{-i\omega_L t}\sigma_+ + \mathcal{O}_\downarrow(\omega_L)\mathrm{e}^{i\omega_L t}\sigma_-. \tag{2.9}$$

The components $\mathcal{O}_{o,z}$ are diagonal in spin space and have spin-angular momentum $s_z = 0$, while correspondingly $\mathcal{O}_{\uparrow,\downarrow}$ are off-diagonal in spin space and have spin-angular momentum $s_z = \pm1$. In Eq. (2.9), we have used the definitions $\sigma_\pm = (\sigma_x \pm i\sigma_y)/2$.

3. Andreev-reflection-induced spin torques

Quasiparticle scattering in a Josephson junction may lead to the formation of Andreev levels if the scattering occurs in such that a way that the quasiparticles interfere constructively (see Fig. 1(b)). In the presence of a precessing spin, the quasiparticle scattering is modified by processes shown in Fig. 1(c); a tunnelling quasiparticle may gain (lose) energy ω_L while simultaneously flipping its spin from down (up) to up (down). The Andreev level spectrum essentially depends on the ratio between the hopping amplitudes, $\mathrm{v_o}/\mathrm{v_s}$. If $\mathrm{v_o}/\mathrm{v_s} < (>)1$, the junction is in a $\pi(0)$ state [52,53], see

Fig. 1(d). The additional precession-induced tunnelling processes modify the Andreev levels. The Larmor frequency, ω_L, determines the amount of energy exchanged during a tunnelling event, while the cone angle, ϑ, determines the amount of scattering between the spin-up and -down bands. These parameters, as well as the temperature, determine the population of the Andreev states [53,54]. In Figure 2, we summarise how the tunnelling over a precessing spin modifies the Andreev spectra by introducing scattering resonances created by the combination of quanta exchange of $\hbar\omega_L$ and spin flips. The charge current is time-independent but still dependent on both ω_L and ϑ as seen in Fig. 2. While the Josephson effect over the precessing spin is interesting in its own right, we will not discuss the current-phase relations further in this paper and refer the interested reader to the original articles [52–54]. Instead, we will focus on the effects of dynamic spin-triplet correlations and their consequences.

An s-wave superconductor contains only spin-singlet correlations $\sim \frac{1}{2}\langle\psi_\uparrow\psi_\downarrow - \psi_\downarrow\psi_\uparrow\rangle$ and can not support a spin current. Nevertheless, induced spin-triplet correlations can be formed due to spin mixing and locally broken spin-rotation symmetry [11,26,60]. The rotation of the classical spin generates new spinful correlations and spin currents that are created by the Andreev processes depicted in figure 1(b-c); positive interference along closed loops leads to the spin-triplet correlations $\frac{1}{2}\langle\psi_\uparrow\psi_\downarrow + \psi_\downarrow\psi_\uparrow\rangle$, $\langle\psi_\uparrow\psi_\uparrow\rangle$ and $\langle\psi_\downarrow\psi_\downarrow\rangle$. These correlations depend on the characteristics of the tunnelling interface, i.e. the precession frequency, ω_L, the cone angle, ϑ, the relative amplitude of hopping strengths, $\mathrm{v_o}, \mathrm{v_s}$, as well as the superconducting phase difference φ, and the temperature, T. These spin-triplet correlations are localised near the junction interface and decay over length scales on the order of the superconducting coherence length [43,61].

The spin-singlet components can be quantified by $\psi(\hat{k}) = \int_{-\varepsilon_c}^{\varepsilon_c} d\varepsilon[f^<(\hat{k},\varepsilon) + f^<(-\hat{k},\varepsilon)]/8\pi i$, where $f^<(\pm\hat{k},\varepsilon)$ denotes the anomalous Green's functions at the Fermi-surface points $\pm\hat{k}$. $\psi(\hat{k})$ is a measure of the (singlet) pairing correlations available to form a singlet order parameter $\Delta_s(\hat{k}) = \lambda_s\eta(\hat{k})\langle\eta(\hat{k}')\psi(\hat{k}')\rangle_{\hat{k}'\cdot\hat{n}>0}$, where $\eta(\hat{k}) = \eta(-\hat{k})$ are basis functions of even parity on which the pairing interaction may be expanded and $\hat{n}$ is the direction of the surface normal. The energy ε_c is the usual cut-off that appears in the BCS gap equation. The triplet correlations span the spin space in such a way that $\boldsymbol{f}_z^< \sim \frac{1}{2}\langle\psi_\uparrow\psi_\downarrow + \psi_\downarrow\psi_\uparrow\rangle$ and $\boldsymbol{f}_{\uparrow/\downarrow}^< \sim \langle\psi_{\uparrow/\downarrow}\psi_{\uparrow/\downarrow}\rangle$. We quantify the induced spin-triplet correlations, $\boldsymbol{f}^<$, in terms of a $\boldsymbol{d}$ vector, which in general is a 2×2 triplet order parameter given by $\Delta_{\hat{k}} = \boldsymbol{d}(\hat{k})\cdot\boldsymbol{\sigma}\, i\sigma_y$ and points along the direction of zero spin projection of the Cooper pairs [62]. We make the following definitions:

$$\pi \text{ junctions} \qquad \boldsymbol{d}_o(\hat{k}) = \hat{n}\cdot\hat{k}\int_{-\varepsilon_c}^{\varepsilon_c}\frac{d\varepsilon}{8\pi i}[\boldsymbol{f}^<(\hat{k},\varepsilon) - \boldsymbol{f}^<(-\hat{k},\varepsilon)], \tag{3.1a}$$

$$0 \text{ junctions} \qquad \boldsymbol{d}_e(\hat{k}) = \int_{-\varepsilon_c}^{\varepsilon_c}\frac{d\varepsilon}{8\pi i}s_\varepsilon[\boldsymbol{f}^<(\hat{k},\varepsilon) + \boldsymbol{f}^<(-\hat{k},\varepsilon)], \tag{3.1b}$$

where the vector $\boldsymbol{d}_o$ is odd in momentum and even in energy, and the vector $\boldsymbol{d}_e$ is even in momentum and odd in energy. s_ε is the sign of the energy ε. Spin-triplet pairing that is *even-in* $\hat{k}$ and *odd-in* ε was first considered as a candidate pairing state for ^{3}He [63] and has recently been realised in superconductor/inhomogeneous magnet interfaces [64]. The time-dependence of the $\boldsymbol{d}$ vector follows from Eqs. (2.8), (2.9), i.e.

$$\boldsymbol{d}(t) = \boldsymbol{d}_z + \boldsymbol{d}_\uparrow e^{-i\omega_L t} + \boldsymbol{d}_\downarrow e^{i\omega_L t}. \tag{3.2}$$

For $\mathrm{v_o} = 0$ and finite $\mathrm{v_s}$, the components are equal in magnitude, $\boldsymbol{d}_\uparrow = \boldsymbol{d}_\downarrow = -\boldsymbol{d}_z$ and scale with a common prefactor, $\mathcal{D}_s\omega_L$, where $\mathcal{D}_s = 4{\mathrm{v_s}}^2/[1 + 2({\mathrm{v_o}}^2 + {\mathrm{v_s}}^2) + ({\mathrm{v_o}}^2 - {\mathrm{v_s}}^2)^2]$. As expected, the $\boldsymbol{d}$-vector components decrease for increasing temperature until they vanish at $T = T_c$. For finite values of $\mathrm{v_o}$, the universal scaling disappears and the $\boldsymbol{d}$-vector components display an asymmetry between $\boldsymbol{d}_\uparrow$ and $\boldsymbol{d}_\downarrow$. For temperatures $T/T_c \lesssim 0.1$, the $\boldsymbol{d}$ vector can be expressed in terms of the classical spin,

$$\boldsymbol{d}(t) = \delta_L\dot{\boldsymbol{S}}(t)\times\boldsymbol{S}(t) + \delta_H(\gamma\boldsymbol{H})\times\boldsymbol{S}(t) + \delta_z\boldsymbol{S}_z. \tag{3.3}$$

For the odd $\boldsymbol{d}$ vector, $\delta_{z,o} = 0$ and, in the tunnel limit at zero temperature, $\delta_{L,o} = \pi\mathcal{D}_s\sin(\varphi/2)$ and $\delta_{H,o} = 4\pi i\mathrm{v_o}\mathrm{v_s}\sin(\varphi/2)$. The $\boldsymbol{d}$ vectors in the left and right leads are related by $\boldsymbol{d}_R(t) = -\boldsymbol{d}_L(t)$.

The spin-vector part of the normal Green's function, $\boldsymbol{g}^{R/A}$, can be expressed in terms of the spin-vector part of the anomalous Green's functions, $\boldsymbol{f}^{R/A}$, using the normalisation condition. In the limit of a small cone angle, the z component is negligible and

$$g^{R(A)}_{\uparrow/\downarrow,\alpha}\left(\varepsilon \mp \frac{\omega_L}{2}\right) = \frac{1}{\bar{g}^{+/-,R(A)}_{s,\alpha}}\left\{\left[\frac{(1\pm i)}{2} f^{R(A)}_{s,\alpha}\left(\varepsilon \pm \frac{\omega_L}{2}\right) + \frac{(1\mp i)}{2} f^{R(A)}_{s,\alpha}(\varepsilon)\right]\tilde{f}^{R(A)}_{\uparrow/\downarrow,\alpha}(\varepsilon) + \left[\frac{(1\mp i)}{2}\tilde{f}^{R(A)}_{s,\alpha}\left(\varepsilon \pm \frac{\omega_L}{2}\right) + \frac{(1\pm i)}{2}\tilde{f}^{R(A)}_{s,\alpha}(\varepsilon)\right] f^{R(A)}_{\uparrow/\downarrow,\alpha}(\varepsilon)\right\}, \quad (3.4)$$

where $\bar{g}^{+/-,R(A)}_{s,\alpha} = g^{R(A)}_{s,\alpha}(\varepsilon) + g^{R(A)}_{s,\alpha}(\varepsilon \pm \omega_L/2)$ and $g^{R(A)}_{x,\alpha} = [g^{R(A)}_{\uparrow,\alpha} + g^{R(A)}_{\downarrow,\alpha}]/2$ and $g^{R(A)}_{y,\alpha} = i[g^{R(A)}_{\uparrow,\alpha} - g^{R(A)}_{\downarrow,\alpha}]/2$.

It is then clear that the existence of the spin currents, $\boldsymbol{j}^s_\alpha = (1/4)\int(d\varepsilon/8\pi i)\mathrm{Tr}\{\hat{\tau}_3\hat{\boldsymbol{\sigma}}[\hat{g}^{i,K}_\alpha(\varepsilon,t) - \hat{g}^{o,K}_\alpha(\varepsilon,t)]\}$, are a direct consequence of the precession-induced spin-triplet correlations. See also Appendix in Ref. [54]. Unfortunately, the spin currents decay over relatively short distances, viz. the superconducting coherence length, and are therefore difficult to measure. The spin current is nothing but transport of spin-angular momentum and the non-conservation of the spin current results in a torque acting on the rotating spin thereby creating a back-action on the precessing spin that is sufficiently large for experimental detection [53], as will be described below.

Since $\boldsymbol{j}^s_R(t,\varphi) = -\boldsymbol{j}^s_L(t,-\varphi) \neq \boldsymbol{j}^s_L(t,\varphi)$, the difference between the spin currents can be used to calculate the torque $\boldsymbol{\tau}(t)$ in Eq. (2.1). We call this torque the Andreev torque since it has its origin in the Andreev scattering processes described in Fig. 1. The torque contribution per conduction channel is

$$\boldsymbol{\tau}_A(t) = \frac{2\hbar}{S}\mathcal{D}_s\beta_H\cos\vartheta\,(\gamma\boldsymbol{H})\times\boldsymbol{S}(t). \quad (3.5)$$

This torque describes a shift of the precession frequency, $\omega_L \to \omega_L[1 + \frac{2\hbar}{S}\mathcal{D}_s\beta_H\cos\vartheta]$, and this shift is therefore a direct consequence of the induced spin-triplet correlations.

A measurement of this frequency shift is a measurement of the induced spin-triplet correlations. Since the shift is $\propto 1/S$, we suggest a nanomagnet with a spin that is small, but still large enough to be treated as a classical spin, say a magnetic nanoparticle with spin $S \sim 50\hbar$. For a contact with two superconducting niobium (Nb) leads, the effective contact area is $\sim \pi\xi_0^2$, where the superconducting coherence length $\xi_0 \sim 40$ nm for Nb. A contact width of ~ 40 nm contains $n \sim 200$ conduction channels. In bulk Nb, $\Delta \sim 1$ meV, but can be made considerably smaller in the point contact, say $\Delta \sim 200\,\mu$eV. We can now study the changes to the precession due to the Andreev torque. In a typical FMR experiment, the resonance peak in the power absorption spectrum has a width that is produced by inhomogeneous broadening, e.g. from anisotropy fields, and homogeneous broadening, which is due to Gilbert damping, and can be expressed as $\Delta H_{\mathrm{hom}} = \frac{2}{\sqrt{3}}H\alpha_G$ [65], where $H = |\boldsymbol{H}|$ and $\alpha_G = \frac{2\hbar}{S}n\alpha\mathcal{D}_s$ is the Gilbert constant [30]. A typical magnetic field is $H \sim 180$ mT, which corresponds to a Larmor precession of $\sim 20\,\mu$eV or 5 GHz. Here, we have assumed a uniform precessional motion. In Ref. [53], it was shown that the normal quasiparticles freeze out as the temperature is lowered. This process results in a decrease of the width of the resonance peak [66]. For a junction with $\mathcal{D}_s \sim 0.1$, the difference in homogeneous broadening is on the order of $\Delta H_{\mathrm{hom}}(T/T_c > 1) - \Delta H_{\mathrm{hom}}(T/T_c \to 0) \sim 80$ mT. In addition to the resonance peak width reduction, the shift of the resonance peak H_0 due to the Andreev torque appears. The frequency shift corresponds to $\Delta\omega_L/\omega_L = \alpha_G\beta_H\cos\vartheta$. In the tunnel limit, $\beta_H \sim \frac{1}{16}\frac{\omega_L}{\Delta}$ in the low temperature limit [53]. In this limit, a spin with angle $\vartheta = \pi/4$ can hence generate a displacement of the resonance peak by $\Delta H_0/H_0 \sim 2\%$. By increasing the junction transparency, the ratio $\hbar n/S$, or the ratio ω_L/Δ, the ratio $\Delta H_0/H_0$ can be improved.

4. Spin-precession assisted multiple Andreev reflection

Replacing the phase bias by a voltage bias (Fig. 3(a)) leads to several new features [55] attributable to the interplay between the time-dependent $\boldsymbol{d}$ vectors and the Josephson frequency, $\omega_J =$

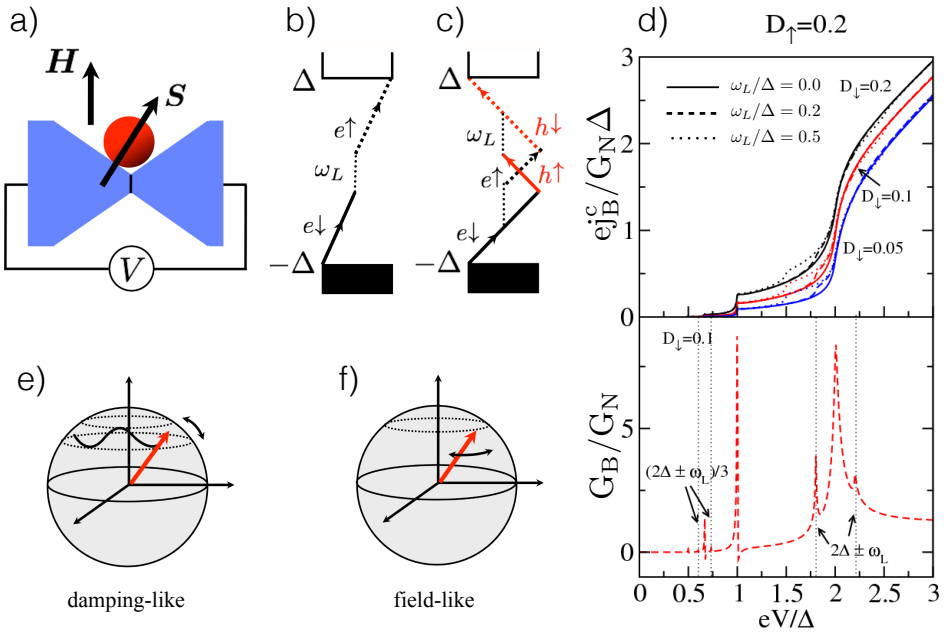

Figure 3. (a) Same setup as in Fig. 1 but with a bias voltage applied across the tunnel junction. The (b) first- and (c) second-order MAR processes combined with absorption of energy ω_L. (d) Current-voltage characteristics for the dc charge current j_B^c (top) and differential conductance (bottom), $G_B = \partial j_B^c/\partial V$, normalised by the normal conductance $G_N = [e^2/h][\mathcal{D}_\uparrow + \mathcal{D}_\downarrow]$. In both plots, $\vartheta = \pi/8$. Sketches of the time-dependent (e) damping-like and (f) field-like torques created by spin-precession-assisted MAR.

$2eV/\hbar$. The replacement causes the phase difference to increase linearly in time, $\varphi(t) = \varphi_0 + \omega_J t$, where φ_0 is the initial phase difference. The bias voltage in combination with energy exchange with the precessing spin creates multiple Andreev reflection (MAR) processes that lead to characteristic signatures in the charge current-voltage characteristics [47,67–69]. Two examples of spin-precession-assisted MAR are shown in Fig. 3. Similarly to the phase-biased case, energy absorption (emission) corresponds to spin flip from down (up) to up (down). The first-order process shown in Fig. 3(b), which includes an energy absorption of ω_L, leads to a contribution to the IV characteristics at the energy $eV = 2\Delta - \omega_L$. Fig. 3(c) shows the two possible second-order processes that include absorption of energy. The spin flip associated with the energy exchange introduces a minus sign in the next Andreev-reflection amplitude due to the change between the spinors $(\psi_\uparrow, \psi_\downarrow^\dagger)^T \leftrightarrow (\psi_\downarrow, \psi_\uparrow^\dagger)^T$. This sign difference leads to destructive interference and suppression of the total Andreev reflection. Destructive interference occurs for all even processes, $n = 2, 4, ...$, while higher-order odd processes display constructive interference.

The bias voltage makes the calculations of the charge and spin currents considerably more complicated. This complication arises in large due to the MAR processes, which make it impossible to express the Green's functions using a closed set of equations. Instead, a recursive approach, see Ref. [55] for details, has to be used. The general time dependence of a general matrix such as $\check{X}(t, t')$ in Eq. (2.8) now has to be complemented by the time dependence generated by the Josephson frequency. In general, the current is given by

$$j_\alpha^\mu(t) = \sum_{n,m} e^{-i(n\varphi_0 + m\chi_0) - i(n\omega_J + m\omega_L)t} (j_\alpha^\mu)_n^m \,. \tag{4.1}$$

The current components are

$$(j_\alpha^\mu)_n^m = \int \frac{d\varepsilon}{4} \mathrm{Tr}\{\hat{\kappa}^\mu [\check{t}(\varepsilon + n\omega_J + m\omega_L)\check{g}(\varepsilon) - \check{g}(\varepsilon + n\omega_J + m\omega_L)\check{t}(\varepsilon + n\omega_J + m\omega_L)]^<\}, \quad (4.2)$$

where we have defined $\hat{\kappa}^0 = e\hat{\tau}_3$ for the charge current and $\hat{\kappa}^i = \mathrm{diag}(\sigma_i, \sigma_y\sigma_i\sigma_y)/2$ for a spin current with a polarisation in the $i = x, y, z$ direction. Note that just as the current depends on the initial phase φ_0, it also depends on χ_0, which is the initial value of the in-plane projection of the precessing spin. The integer m takes the values $\{-1, 0, 1\}$ corresponding to $\{\downarrow, d, \uparrow\}$ in Eq. (2.8). Defining $\mathrm{v}_{\uparrow/\downarrow} = \mathrm{v_o} \pm \mathrm{v_s}\cos\vartheta$, we write $\mathcal{D}_{\uparrow(\downarrow)} = 4\mathrm{v}_{\uparrow(\downarrow)}^2/[1 + \mathrm{v}_{\uparrow(\downarrow)}^2]^2$.

The dc charge current and the differential conductance, plotted in Fig. 3(d), clearly show the contributions to the current generated by the spin-precession-assisted MAR processes. These features appear at voltages $eV = (2\Delta \pm \omega_L)/n$, where $n = 1, 3, ...$ Note that, as expected, the contributions for the even processes $n = 2, 4, ...$ are absent. It can be shown that the ac charge current only includes harmonics of ω_J, i.e. $j_\alpha^0(t) = \sum_n e^{-in(\varphi_0 + \omega_J t)}(j_\alpha^0)_n^0$. This time dependence is an effect of the combined energy exchange-spin flip tunnelling processes.

The spin current, on the other hand, includes all harmonics of the Larmor and Josephson frequencies. This time dependence is captured by the spin-transfer torque, whose ω_L dependence is described by the expression

$$\boldsymbol{\tau}(t) = \frac{\gamma_H(t)}{S}\gamma \boldsymbol{H} \times \boldsymbol{S} + \frac{\gamma_L(t)}{S^2}\dot{\boldsymbol{S}} \times \boldsymbol{S}, \quad (4.3)$$

where the prefactors, $\gamma_{H/L}$, oscillate with the Josephson frequency, $\gamma_{H/L}(t) = \sum_n \gamma_{H/L,n} e^{in\omega_J t}$. The component $\gamma_{L,0}$ describes a finite shift of the precession angle ϑ, while the term $\propto \gamma_{H,0}$ signals a shift of the precession frequency. The damping-like torque $\propto \gamma_{L,n}$ and the field-like torque $\propto \gamma_{H,n}$ describe Josephson nutations [70] and oscillations of the precession frequency, respectively.

Since the torque (4.3) includes harmonics of both ω_J and ω_L, resonances may occur when the two frequencies are commensurate. These Shapiro resonances occur at the bias voltage $V_n^m = -(m/n)\omega_L/2e$ where $n, m \neq 0$, and results in a dc contribution to the spin-transfer torque and can be seen as a rectification of the higher harmonics of the torque in section 3. As the ac part of the torque (4.3) originates from an in-plane spin-polarised current, one can then conclude that the Shapiro resonances produce dc in-plane torque components. The Shapiro resonances hence break the rotational symmetry around the z axis and, therefore, the Shapiro torque depends on the initial angle of nanomagnet's magnetisation direction, χ_0. This situation is analogous to the φ_0-dependence for the Shapiro steps seen in microwave-irradiated Josephson junctions [71–73].

The dc Shapiro torque will cause the spin to precess around a new z axis. Choosing suitable parameters and applying a self-consistent solution, one finds that the Shapiro torque is able to reverse the spin's direction. To this end, we choose $n = 1$ and optimise the effect of the Shapiro torque by maximising the ratio $\gamma_{H,1}/\gamma_{L,1}$. It was found in Ref. [55] that $\gamma_{H,1}$ strongly depends on the junction transparency but exhibits a weak dependence on the precession angle. We therefore choose $\mathrm{v_o} = 0$, $\mathrm{v_s} = 0.7$, and $\vartheta = 0.1\pi$. We consider a tunnel junction consisting of Nb having a superconducting gap $\Delta \sim 0.5$ meV and containing a magnetic nanoparticle with spin $S \sim 50\hbar$ with a typical frequency $\omega_L \sim 5$ GHz that corresponds to a magnetic field well below the critical magnetic field. We therefore have $\omega_L/\Delta = 0.01$. A magnetic field close to the critical magnetic field reduces Δ and increases the resolution of features depending on the ratio ω_L/Δ, e.g. the subgap features in the dc charge current. A point contact of width ~ 40 nm has ~ 200 conduction channels, which gives an estimated sub-nanosecond switching time for the first Shapiro resonance.

5. Conclusion

We have reviewed recent work on how the magnetisation dynamics of a nanomagnet couple to the charge and spin Josephson effects. The precession of the nanomagnet modifies the Andreev scattering in several ways. First, it introduces a spin-polarised Andreev level spectrum and

dynamical spin-triplet pairing correlations in the vicinity of the junction. Second, it couples in-gap Andreev levels with the continuum part of the spectrum causing a nonequilibrium population of the Andreev levels. Third, it creates a nonequilibrium population of the Andreev levels, leading to Andreev levels carrying current in opposite directions being populated and a strongly modified current-phase relation. We have focused on the consequences of the spin-polarised Andreev-level spectra and how they couple back to the precession dynamics of the nanomagnet via conservation of spin-angular momentum. Depending on if the Josephson junction is phase biased or voltage biased, the this torque can modify the precession frequency, either by a frequency shift or by frequency modulations, or it can introduce nutations. Recent experiments on superconductor/ferromagnet nanojunctions can extract the microscopic details of the scattering and match junction parameters such as spin-filtering and spin-mixing effects [74–76]. If the ferromagnetic part of the junction would be a single domain magnetic grain, properties described in this review could be probed in experiments.

Acknowledgements. C.H. and W.B. were supported by the DFG and SFB 767. M.F. acknowledges support from the Swedish Research Council (VR).

References

1. Eschrig, M., 2011 Spin-polarized supercurrents for spintronics. *Physics Today* **64**, 43.
2. Linder, J. and Robinson, J. W. A., 2015 Superconducting spintronics. *Nature Physics* **11**, 307.
3. Bulaevskii, L. N., Kuzii, V. V., and Sobyanin, A. A., 1977 Superconducting system with weak links and current in the ground state. *Zh. Éksp. Teor. Fiz.* **25**, 314 [*JETP Lett.* **25**, 290].
4. Ryazanov, V. V., Oboznov, V. A., Rusanov, A. Yu.,Veretennikov, A. V., Golubov, A. A., and Aarts, J., 2001 Coupling of two superconductors through a ferromagnet: Evidence for a π-Junction. *Phys. Rev. Lett.* **86**, 2427.
5. Kontos, T., Aprili, M., Lesueur, J., Genêt, F., Stephanidis, B., and Boursier, R. 2002 Josephson junction through a thin ferromagnetic layer: Negative coupling. *Phys. Rev. Lett.* **89**, 137007.
6. Buzdin, A. I., 2005 Proximity effects in superconductor-ferromagnet heterostructures. *Rev. Mod. Phys.* **77**, 935.
7. Bergeret, F. S., Volkov, A. F., and Efetov, K. B., 2001 Enhancement of the Josephson Current by an Exchange Field in Superconductor-Ferromagnet Structures. *Phys. Rev. Lett.* **86**, 3140.
8. Bergeret, F. S., Volkov, A. F., and Efetov, K. B., 2005 Odd triplet superconductivity and related phenomena in superconductor-ferromagnet structures. *Rev. Mod. Phys.* **77**, 1321.
9. Houzet, M. and Buzdin, A. I., 2007 Long range triplet Josephson effect through a ferromagnetic trilayer. *Phys. Rev. B* **76**, 060504(R).
10. Braude, V., and Nazarov, Yu. V., 2007 Fully Developed Triplet Proximity Effect. *Phys. Rev. Lett.* **98**, 077003.
11. Eschrig, M. and Löfwander, T., 2008 Triplet supercurrents in clean and disordered half-metallic ferromagnets. *Nature Physics* **4**, 138.
12. Keizer, R. S., Goennenwein, S. T. B., Klapwijk, T. M., Miao, G., Xiao, G., and Gupta, A. 2006 A spin triplet supercurrent through the half-metallic ferromagnet CrO_2. *Nature* **439**, 825.
13. Khaire, T. S., Khasawneh, M. A., Pratt, Jr., W. P., and Birge, N. O., 2010 Observation of Spin-Triplet Superconductivity in Co-Based Josephson Junctions. *Phys. Rev. Lett.* **104**, 137002.
14. Mai, S., Kandelaki, E., Volkov, A. F., and Efetov, K. B., 2011 Interaction of Josephson and magnetic oscillations in Josephson tunnel junctions with a ferromagnetic layer. *Phys. Rev. B* **84**, 144519.
15. Konschelle, F. and Buzdin, A., 2009 Magnetic moment manipulation by a Josephson current. *Phys. Rev. Lett.* **102**, 017001.
16. Cai, L. and Chudnovsky, E. M., 2010 Interaction of a nanomagnet with a weak superconducting link. *Phys. Rev. B* **82**, 104429.
17. Waintal, X., and Brouwer, P. W., 2001 Current-induced switching of magnetic domains to a perpendicular configuration. *Phys. Rev. B* **63**, R220407.
18. Waintal, X., and Brouwer, P. W., 2002 Magnetic exchange interaction induced by a Josephson current. *Phys. Rev. B* **65**, 054407.
19. Michelsen, J., Shumeiko, V. S., and Wendin, G., 2008 Manipulation with Andreev states in spin active mesoscopic Josephson junctions. *Phys. Rev. B* **77**, 184506.
20. Linder, J. and Yokoyama, T., 2011 Supercurrent-induced magnetization dynamics in a Josephson junction with two misaligned ferromagnetic layers. *Phys. Rev. B* **83**, 012501.

21. Kulagina, I. and Linder, J., 2014 Spin supercurrent, magnetization dynamics, and φ-state in spin-textured Josephson junctions. *Phys. Rev. B* **90**, 054504.
22. Zhao, E. and Sauls, J. A., 2008 Theory of nonequilibrium spin transport and spin-transfer torque in superconducting-ferromagnetic nanostructures. *Phys. Rev. B* **78**, 174511.
23. Shomali, Z., Zareyan, M., and W. Belzig, W., 2011 Spin supercurrent in Josephson contacts with noncollinear ferromagnets. *New J. Phys.* **13**, 083033.
24. Braude, V., and Blanter, Ya. M., 2008 Triplet Josephson Effect with Magnetic Feedback in a Superconductor-Ferromagnet Heterostructure. *Phys. Rev. Lett.* **100**, 207001.
25. Zhu, J.-X., Nussinov, Z., Shnirman. A., and Balatsky, A.V., 2004 Novel spin dynamics in a Josephson junction. *Phys. Rev. Lett.* **92**, 107001.
26. Houzet, M., 2008 Ferromagnetic Josephson junction with precessing magnetization. *Phys. Rev. Lett* **101**, 057009.
27. Yokoyama, T. and Tserkovnyak, Y., 2009 Tuning odd triplet superconductivity by spin pumping. *Phys. Rev. B* **80**, 104416.
28. Petković, I., Aprili, M., Barnes, S. E., Beuneu, F., and Maekawa, S., 2009 Direct dynamical coupling of spin modes and singlet Josephson supercurrent in ferromagnetic Josephson junctions. *Phys. Rev. B* **80**, 220502.
29. Barnes, S. E., Aprili, M., Petković, I., and Maekawa, S., 2011 Ferromagnetic resonance with a magnetic Josephson junction. *Superconductor Science and Technology* **24**, 024020.
30. Gilbert, T. L., 2004 A Phenomenological Theory of Damping in Ferromagnetic Materials. *IEEE Transactions on magnetics* **40**, 3443.
31. Tserkovnyak, Y., Brataas, A., Bauer, G. E. W., and Haplerin, B. I., 2005 Nonlocal magnetization dynamics in ferromagnetic heterostructures. *Rev. Mod. Phys.* **77**, 1375.
32. Zhu, J.-X., and Balatsky, A.V., 2003 Josephson current in the presence of a precessing spin. *Phys. Rev. B* **67**, 174505.
33. Eilenberger, G., 1968 Transformation of Gorkov's equation for type II superconductors into transport-like equations. *Z. Phys.* **214**, 195.
34. Larkin, A.I. and Ovchinnikov, Y. N., 1969 Quasiclassical method in the theory of superconductivity. *Zh. Éksp. Teor. Fiz.* **55**, 2262 [*Sov. Phys. JETP* **28**, 1200].
35. Eliashberg, G. M., 1971 Inelastic Electron Collisions and Nonequilibrium Stationary States in Superconductors. *Zh. Éksp. Teor. Fiz.* **61**, 1254 [*Sov. Phys. JETP* **34**, 668 (1972)].
36. Serene, J. W. and Rainer, D., 1983 The quasiclassical approach to superfluid ^{3}He. *Phys. Rep.* **101**, 21.
37. Zaitsev, A. V., 1984 Quasiclassical equations of the theory of superconductivity for contiguous metals and the properties of constricted microcontacts. *Zh. Éksp. Teor. Fiz.* **86**, 1742 [*Sov. Phys. JETP* **59**, 1015].
38. Shelankov, A. L., 1984 2-particle tunnelling in normal metal-superconductor contact. *Sov. Phys. Solid State* **26**, 981.
39. Millis, A. J., Rainer, D., and Sauls J. A., 1988 Quasiclassical theory of superconductivity near magnetically active interfaces. *Phys. Rev. B* **38**, 4504.
40. Nagai, K. and Hara, J., 1988 Boundary conditions for quasiclassical Green's function for superfluid Fermi systems. *J. Low Temp. Phys.* **71**, 351.
41. Eschrig, M., 2000 Distribution functions in nonequilibrium theory of superconductivity and Andreev spectroscopy in unconventional superconductors. *Phys. Rev. B* **61**, 9061.
42. Shelankov, A. and Ozana, M., 2000 Quasiclassical theory of superconductivity: A multiple-interface geometry. *Phys. Rev. B* **61**, 7077.
43. Fogelström, M., 2000 Josephson currents through spin-active interfaces. *Phys. Rev. B* **62**, 11812.
44. Barash, Y. S., Bobkova, I. V., and Kopp, T., 2002 Josephson current in S-FIF-S junctions: Nonmonotonic dependence on misorientation angle. *Phys. Rev. B* **66**, 140503(R).
45. Zhao, E., Löfwander, T., and Sauls, J. A., 2004 Nonequilibrium superconductivity near spin-active interfaces. *Phys. Rev. B* **70**, 134510.
46. Eschrig, M., 2009 Scattering problem in nonequilibrium quasiclassical theory of metals and superconductors: General boundary conditions and applications. *Phys. Rev. B* **80**, 134511.
47. Cuevas, J. C., Martín-Rodero, A., and Levy Yeyati, A., 1996 Hamiltonian approach to the transport properties of superconducting quantum point contacts. *Phys. Rev. B* **54**, 7366.
48. Cuevas, J. C., and Fogelström, M., 2001 Quasiclassical description of transport through superconducting contacts. *Phys. Rev. B* **64**, 104502.
49. Andersson, M., Cuevas, J. C., and Fogelström, M., 2002 Transport through superconductor/magnetic dot/superconductor structures. *Physica C* **367**, 117.

50. Eschrig, M., Kopu, J., Cuevas, J. C., and Schön, G., 2003 Theory of Half-Metal/Superconductor Heterostructures. *Phys. Rev. Lett.* **90** 137003.
51. Kopu, J., Eschrig, M., Cuevas, J. C., and Fogelström, M., 2004 Transfer-matrix description of heterostructures involving superconductors and ferromagnets. *Phys. Rev. B* **69**, 094501.
52. Teber, S., Holmqvist, C., and Fogelström, M., 2010 Transport and magnetization dynamics in a superconductor/single-molecule magnet/superconductor junction. *Phys. Rev. B* **81**, 174503.
53. Holmqvist, C., Teber, S., and Fogelström, M., 2011 Nonequilibrium effects in a Josephson junction coupled to a precessing spin. *Phys. Rev. B* **83**, 104521.
54. Holmqvist, C., Belzig, W., and Fogelström, M., 2012 Spin-precession-assisted supercurrent in a superconducting quantum point contact coupled to a single-molecule magnet. *Phys. Rev. B* **86**, 054519.
55. Holmqvist, C., Fogelström, M., and Belzig, W., 2014 Spin-polarized Shapiro steps and spin-precession-assisted multiple Andreev reflection. *Phys. Rev. B* **90**, 014516.
56. Holmqvist, C., 2010 Non-equilibrium Effects in Nanoscale Superconducting Hybrid Junctions. Ph.D. thesis, Chalmers University of Technology.
57. Buchholtz, L. J. and Rainer, D., 1979 Quasiclassical boundary conditions for Fermi liquids at surfaces. *Z. Phys. B* **35**, 151.
58. Thuneberg, E. V., Kurkijärvi, J., and Rainer, D., 1981 Quasiclassical theory of ions in ^{3}He. *J. Phys. C* **14**, 5615 (1981).
59. Thuneberg, E. V., Kurkijärvi, J., and Rainer, D., 1984 Elementary-flux-pinning potential in type-II superconductors. *Phys. Rev. B* **29**, 3913.
60. Alidoust, M., Linder, J., Rashedi, G., Yokoyama, T., and Sudbø, A., 2010 Spin-polarized Josephson current in superconductor/ferromagnet/superconductor junctions with inhomogeneous magnetization. *Phys. Rev. B* **81**, 014512.
61. Shevtsov, O. and Löfwander, T., 2014 Spin imbalance in hybrid superconducting structures with spin-active interfaces. *Phys. Rev. B* **90**, 085432.
62. Vollhardt, D. and Wölfle, P. 1990 The superfluid phases of Helium 3. *Taylor and Frances*.
63. V. L. Berezinskii, 1974 New model of anisotropic phase of superfluid He-3 *Pis'ma Zh. Eksp. Teor. Fiz.* **20**, 628 [*JETP Lett.* **20**, 287].
64. Di Bernardo, A., Diesch, S., Gu, Y., Linder, J., Divitini, G., Ducati, C., Scheer, E., Blamire, M. G., and Robinson, J. W. A. 2015 Signature of magnetic-dependent gapless odd frequency states at superconductor/ferromagnet interfaces. *Nat. Commun.* **6**, 8053.
65. Platow, W., Anisimov, A. N., Dunifer, G. L., Farle, M., and Baberschke, K., 1998 Correlations between ferromagnetic-resonance linewidths and sample quality in the study of metallic ultrathin films. *Phys. Rev. B* **58**, 5611.
66. Bell, C., Milikisyants, S., Huber, M., and Aarts, J., 2008 Spin Dynamics in a Superconductor-Ferromagnet Proximity System. *Phys. Rev. Lett.* **100**, 047002.
67. Octavio, M., Tinkham, M., Blonder, G. E., and Klapwijk, T. M., 1983 Subharmonic energy-gap structure in superconducting constrictions. *Phys. Rev. B* **27**, 6739.
68. Bratus, E. N., Shumeiko, V.S., and Wendin, G., 1995 Theory of Subharmonic Gap Structure in Superconducting Mesoscopic Tunnel Contacts. *Phys. Rev. Lett* **74**, 2110.
69. Averin, D. and Bardas, A., 1995 ac Josephson Effect in a Single Quantum Channel. *Phys. Rev. Lett* **75**, 1831.
70. Nussinov, Z., Shnirman, A., Arovas., D. P., Balatsky, A.V., and Zhu. J. X., 2005 Spin and spin-wave dynamics in Josephson junctions. *Phys. Rev. B* **71**, 214520.
71. Cuevas, J.C., Heurich, J., Martín-Rodero, A., Levy Yeyati, A., and Schön, G., 2002 Subharmonic Shapiro Steps and Assisted Tunneling in Superconducting Point Contacts. *Phys. Rev. Lett* **88**, 157001.
72. Uzawa, Y. and Wang, Z., 2005 Coherent Multiple Charge Transfer in a Superconducting NbN Tunnel Junction. *Phys. Rev. Lett* **95**, 017002.
73. Chauvin, M., vom Stein, P., Pothier, H., Joyez, P., Huber, M. E., Esteve, D., and Urbina, C., 2006 Superconducting Atomic Contacts under Microwave Irradiation. *Phys. Rev. Lett* **97**, 067006.
74. Quay, C. H. L., Chevallier, D., Bena, C., and Aprili, M., 2013 Spin imbalance and spin-charge separation in a mesoscopic superconductor. *Nature physics* **9**, 84.
75. Hübler, F., Wolf, M. J., Beckmann, D., and von Löhneysen, H., 2012 Long-Range Spin-Polarized Quasiparticle Transport in Mesoscopic Al Superconductors with a Zeeman Splitting *Phys. Rev. Lett* **109**, 207001.
76. Wolf, M. J., Hübler, F., Kolenda, S., von Löhneysen, H., and Beckmann, D., 2013 Spin injection from a normal metal into a mesoscopic superconductor. *Phys. Rev. B* **87**, 024517.